

# $^{56}\text{Ni}$ dredge-up in Supernova 1987A

A.Fassia<sup>1</sup> and W.P.S. Meikle<sup>1</sup>

<sup>1</sup>Astrophysics Group, Blackett Laboratory, Imperial College, Prince Consort Rd , London SW7 2BZ, UK

## Abstract

We use early-time observations of He I 10830 Å to measure the extent of upward mixing of radioactive material in SN 1987A. This work develops and extends the work of Graham (1988), and places constraints on actual explosion models. The presence of the He I 10830 Å ( $2s^3S-2p^3P$ ) line at  $\geq 10$  days post-explosion implies re-ionisation by  $\gamma$ -rays from upwardly-mixed radioactive material produced during the explosion. Using the unmixed explosion model 10H (Woosley 1988) as well as mixed versions of it, we estimated the  $\gamma$ -ray energy deposition by applying a purely absorptive radiative transfer calculation. The deposition energy was used to find the ionisation balance as a function of radius, and hence the  $^{25}\text{S}$  population density profile. This was then applied to a spectral synthesis model and the synthetic spectra were compared with the observations. Neither model 10H nor the mixed version, 10HMM, succeeded in reproducing the observed He I 10830 Å line. The discrepancy with the data found for 10HMM is particularly significant, as this model has successfully reproduced the X-ray and  $\gamma$ -ray observations and the UVOIR light curve. We find that a match to the He I line profile is achieved by *reducing* the extent of mixing in 10HMM. Our reduced-mixing models also reproduce the observed  $\gamma$ -ray line light curves and the iron-group velocities deduced from late-time infrared line profiles. We suggest that the He I line method provides a more sensitive measure of the extent of mixing in a type II supernova explosion.

**Key words::**supernova,  $\gamma$  rays, mixing, infrared ,spectra, 87A

# 1 Introduction

It has long been recognised (Falk & Arnett 1973) that hydrodynamic instabilities should occur in type II supernova explosions. Chevalier (1976) studied the stability of shocks propagating through simple power-law density distributions and showed that for some cases the matter behind the shock is subject to instabilities. Bandiera (1984) further emphasised the role of such instabilities in generating chemical mixing.

SN 1987A provided the first observational evidence for extensive mixing of the ejecta. Simple stratified models did not account for the extended, smooth, rounded plateau in the UVOIR light curve which was observed during the era covering 25 to 125 days post-explosion. To successfully model the light curve, it proved necessary to invoke upward mixing of radioactive nickel and cobalt to high velocities together with downward mixing of hydrogen deep into the core (Arnett 1988, Woosley 1988, Shigeyama *et al.* 1988, Shigeyama & Nomoto 1990, Nomoto *et al.* 1998). Upward mixing of radioactive  $^{56}\text{Ni}$  and  $^{56}\text{Co}$  to the outer regions of the envelope was also indicated by the early detection of X-rays (*e.g.* Dotani *et al.* 1987, Sunyaev *et al.* 1987) and  $\gamma$ -rays (*e.g.* Matz *et al.* 1988, Mahoney *et al.* 1988, Sandie *et al.* 1988, Cook *et al.* 1988). Furthermore, the expansion velocities inferred from the line widths of infrared spectral lines of Fe II and Co II (Spyromilio, Meikle & Allen 1990, Haas *et al.* 1990, Tueller *et al.* 1990) indicated that a fraction of the iron-group elements had been dredged up to velocities as high as  $\sim 3000$  km/s.

These observations stimulated the modelling of explosions both in two dimensions (Arnett *et al.* 1989, Hachisu *et al.* 1990, Fryxell *et al.* 1991) and three dimensions (Müller *et al.* 1991). This theoretical work showed that significant mixing occurs as the explosion shock plows through the ejecta. However, the maximum iron-group velocities derived did not exceed 1300 km/s. This discrepancy with the observations was attributed to non-inclusion in the models of the radioactive decay energy deposited in the ejecta. Herant & Benz (1991) included the radioactive decay energy in their two-dimensional code, resulting in the formation of a giant “nickel bubble” during the first few weeks. In spite of this, their model still only attained iron-group velocities up to  $\sim 2000$  km/s - 1000 km/s less than that indicated by the observed iron-group line profiles.

Herant & Benz (1992) excluded the possibilities that the velocity discrepancy was due to three-dimensional effects, errors in the adopted progenitor structure, or numerical resolution. They argued that in order to explain the observed high velocities, it was necessary to invoke mixing during the early stages of the explosion when nickel is created by explosive nucleosynthesis (Herant *et al.* 1994). By *pre-mixing* nickel out to  $1.5 M_{\odot}$  above the mass cut, they found that the subsequent Rayleigh-Taylor instabilities could produce iron-group velocities as high as those observed. Such pre-mixing is possible within the context of the delayed explosion mechanism (Herant, Benz, & Colgate (1992); Herant *et al.* 1994). In this scenario, the explosion is driven by neutrinos from the proto-neutron star which deposit energy in material just above the neutrinosphere, producing a hot, high-entropy bubble interior to low-entropy shocked matter. This

situation is prone to strong convective motions under the influence of the gravitational pull of the proto-neutron star, thus breaking the spherical symmetry. The residual inhomogeneities due to these early instabilities may be sufficient to seed subsequent shell-interface Rayleigh-Taylor instabilities.

Another way to account for the observed high velocities is through the effect of a spherically symmetric shock on irregularities or “seeds” formed in the  $^{16}\text{O}$  burning shell before core-collapse. Recent hydrodynamic calculations (Bazan & Arnett 1998, Arnett 1994) have shown that the oxygen burning is intermittent, chaotic and strongly localised. The heterogeneous composition developed provides “seed” perturbations in density. These are believed to be sufficiently large to produce hydrodynamic instabilities which cause mixing in the presupernova envelope. This occurs in precisely the region where  $^{56}\text{Ni}$  is explosively produced by oxygen burning behind the explosion shock. However, quantitative results are not yet available.

To test the possible mixing mechanisms described above we need to be able to probe the conditions deep inside the supernova. In principle, much can be learned from the  $\gamma$ -ray and X-ray light curves. In addition, once the ejecta have become optically thin ( $t \geq 150$  days), high signal-to-noise infrared spectral line profiles of heavy elements can provide a powerful probe of their spatial distribution, and degree of mixing (Spyromilio, Meikle & Allen 1990, Herant & Woosley 1994). Unfortunately, apart from the exceptionally close SN 1987A, current instruments are insufficiently sensitive to allow such studies to be made for typical nearby type II supernovae.

An interesting alternative is to probe the mixing of the nickel using infrared spectra at early times. This approach was first presented by Graham (1988), and was developed further by us (Fassia *et al.* 1998). The method is based on the detection and modelling of the He I 10830 Å ( $2s^3\text{S}-2p^3\text{P}$ ) line. This is a high excitation line. It is formed in a region where the population of the metastable  $2s^3\text{S}$  level is maintained by the balance of the recombination rate of  $\text{He}^+$  with the rates of collisional de-excitation and forbidden radiative decay. However, because the  $\text{He}^+$  recombination timescale is  $< 1$  d (Graham 1988) we expect that at late times ( $t > 10$  d) all helium should be neutral and in its ground state. Thus, if He I 10830 Å is present at times after 10 d there must exist a re-ionising mechanism. The identification of this line well after 10 d in SNe 1987A and 1995V led Graham (1988) and Fassia *et al.* (1998) to propose that the ionisation was maintained by the  $\gamma$ -rays emitted from the decay of  $^{56}\text{Ni}/^{56}\text{Co}$ . The subsequent recombination produces the He I 10830 Å line. Owing to the exponential sensitivity of the  $\gamma$ -ray flux to the column depth (Pinto & Woosley 1988) the observed He I line profile is sensitive to the amount of radioactive material moving at high velocities. Thus, the He I 10830 Å line can probe the extent of upward mixing or “dredge-up” of iron-group elements in a type II supernova. This was demonstrated by Fassia *et al.* (1998) for the type IIp supernova SN 1995V. While an unmixed explosion model did not reproduce the observed He I line, by invoking upward mixing of about  $10^{-6} M_{\odot}$  of  $^{56}\text{Ni}$  to velocities above 4000 km/s (i.e. above the helium photosphere) we were able to match the observed spectra.

In the present work we use the He I line method to carry out a detailed study of the

dredge-up of radioactive material in the ejecta of SN 1987A, and to place constraints on possible mixing models. The method is described in section 2. In section 3 we present results from the comparison of theoretical models with the data and estimate the  $^{56}\text{Co}$  dredge-up. We also compare our predictions of  $\gamma$ -ray fluxes with the observed  $\gamma$ -ray light curves. In section 4 we discuss the implications of this work in constraining and understanding the dredge-up.

## 2 Determination of $^{56}\text{Ni}$ dredge-up in SN 1987A using the He I 10830 Å line

In spectra of SN 1987A obtained in the period 76-135 days post-explosion, Elias *et al.* (1988) and Meikle *et al.* (1989) identified a strong absorption feature at  $\sim 10,700$  Å with the blue-shifted P Cygni trough of He I 10830 Å. Using the spectral synthesis model described in Fassia *et al.* (1998), where the lines are formed by pure scattering above the photosphere and where line blending is taken into account, we have confirmed this identification and shown that the He I line was blended with C I 10695 Å. The He I line trough was blueshifted by about 5000 km/s. This is in sharp contrast to other infrared P Cygni lines where velocities of less than 2000 km/s were observed (Elias *et al.* 1988, Meikle *et al.* 1989). The high blueshift and depth of the trough indicate that the line was optically thick, and formed in the outermost layers of the expanding supernova envelope.

As explained above, the presence of the He I line implies re-ionisation by the  $\gamma$ -rays of  $^{56}\text{Co}$ . Modelling of the He I line profile and evolution was carried out as follows. We began with the unmixed explosion model 10H (Woosley 1988), calculated the radioactive energy deposited in the outer envelope of the supernova and hence found the ionisation balance as a function of radius. We then determined the  $2s^3S$  population density profile. This was fed into our spectral synthesis model and the synthetic line profile was compared with the observations. As will be shown below, model 10H drastically underproduced the He I 10830 Å feature, suggesting that upward mixing of radioactive material must have occurred during the explosion. To determine the degree of this dredge-up we gradually increased the mixing of the  $^{56}\text{Co}$  until a match with the observations was obtained.

### 2.1 Calculation of the energy deposition and the emergent luminosity of the $\gamma$ -rays

$\gamma$ -ray energy deposition was computed by performing a radiation transport solution for each  $\gamma$ -ray line produced in the decay  $^{56}\text{Co} \rightarrow ^{56}\text{Fe}$ . Line energies and emission probabilities were obtained from Lederer & Shirley (1978). We also included  $\gamma$ -rays from the annihilation of positrons emitted in 19% of the  $^{56}\text{Co}$  decays. For this reason, following Leising & Share (1990), we used a branching ratio of 0.38 for  $\gamma$ -rays with

energies of 0.511 MeV.

We estimated the  $\gamma$ -ray energy deposition and the escape fractions, using a purely absorptive transfer equation. While Monte Carlo simulations provide the most realistic and physically accurate description of the  $\gamma$ -ray energy deposition, they are excessively demanding of computational resources. In contrast, the radiative transfer method, adopted in this study, is computationally efficient and has been shown to give results reasonably close to those obtained by the Monte Carlo techniques (Swartz *et al.* 1995). This is because the  $\gamma$ -ray energies are such that Compton scattering dominates. The ratio of scattered to incident photon energies is given by

$$\frac{E'_\nu}{E_\nu} = \frac{1}{1 + (E_\nu/m_e c^2)(1 - \cos \theta)} \quad (1)$$

where  $E_\nu$  is the initial photon energy, and  $E'_\nu$  is photon energy after it scatters from an electron at rest through angle  $\theta$ . Thus the energy transferred in a single scatter can be large *e.g.* a  $\sim 2$  MeV  $\gamma$ -ray photon gives up  $\geq 0.8$  of its energy when it scatters through  $\theta \geq 90^\circ$  (Swartz *et al.* 1995). Even though the scattering cross section is forward peaked, forward-scattering transfers very little energy to the gas. Therefore, one can think of the  $\gamma$ -ray line photon as travelling along a linear path until it suffers a large-angle scatter, at which point it gives up most of its energy and becomes a “continuum” photon. Consequently, in calculating the line transfer, the Compton scattering can be treated as producing a purely absorptive opacity. Thus, the radiative transfer equation is linear for the  $\gamma$ -ray lines. We can therefore calculate the energy deposition and escape intensities by direct integration of the radiative transfer equation. The emissivity for this calculation is given by the local volume rate of  $\gamma$ -ray production. Following Woosley’s *et al.* (1994) approach, the opacity is assumed to consist of scattering and absorptive parts. The scattering component is

$$\kappa_{scat}^\nu = \frac{N_e \sigma_{KN}(E_\nu)}{1 + (E_\nu/m_e c^2)(1 - \cos \theta_{scat})} \quad (2)$$

and the absorptive part is:

$$\kappa_{abs}^\nu = N_e \sigma_{KN}(E_\nu) \left[ 1 - \frac{1}{1 + (E_\nu/m_e c^2)(1 - \cos \theta_{scat})} \right] \quad (3)$$

where  $E_\nu$  is the initial photon energy,  $N_e$  is the total (bound and free) electron density,  $\sigma_{KN}(E_\nu)$  is the Klein-Nishina cross section, and  $\theta_{scat}$  is the scattering angle. In our calculations we have followed (Woosley *et al.* 1994) in assuming that all photons scatter through the same angle,  $\theta_{scat}=90^\circ$ . This assumption gives results that agree to within a few percent with those obtained from more detailed Monte-Carlo calculations.

The code solves the frequency dependent equations of radiative transfer by integrating along impact parameters parallel to the observer’s line of sight (see Figure 1). Following Swartz *et al.* (1995) the transfer equation in the “(p,z) representation” along a ray is:

$$\pm \frac{\partial I_\nu^\pm}{\partial z}(p, z) = \eta_\nu - \kappa_\nu(r) I_\nu^\pm \quad (4)$$

where  $I^+$  ( $I^-$ ) denotes the outgoing (ingoing) radiation,  $z$  is the position along the ray (Figure 1) and  $\eta_\nu = f_{rad}s_\gamma(E_\nu)\rho/4\pi$  is the local  $\gamma$ -ray emissivity. Here,  $f_{rad}$  is the initial mass fraction of  $^{56}\text{Ni}$ ,  $\rho$  is the mass density and  $s_\gamma(E_\nu)$  is the time-dependent rate of energy release per gram of radioactive material:

$$s_\gamma(E_\nu) = \frac{1.25 \times 10^{17} E_\nu b_{E_\nu} e^{\frac{-t}{\tau_{Co}}}}{\tau_{Co}} (\text{erg } g_{rad}^{-1} \text{ s}^{-1}) \quad (5)$$

where  $b_{E_\nu}$  is the branching ratio for a line of energy  $E_\nu$ , and  $\tau_{Co}$  is the mean life time of  $^{56}\text{Co}$  ( $\tau_{Co}=113.7$  days). Introducing the optical depth along the ray,  $d\tau = -\kappa_\nu dz$ , the equation of transfer becomes:

$$\mp \frac{dI_\nu^\pm}{d\tau} = -\frac{\eta_\nu}{\kappa_\nu} + I^\pm. \quad (6)$$

If we now take into account that  $N_e = (\rho/m_u)Y_e$  where  $m_u$  is the atomic mass unit and  $Y_e$  is the total number of electrons per baryon, we have:

$$\mp \frac{d\mathcal{I}_\nu^\pm}{d\tau} = -\frac{f_{rad}}{Y_e} + \mathcal{I}^\pm \quad (7)$$

where

$$\mathcal{I} = \left( \frac{4\pi\kappa_\nu}{s_\gamma m_u N_e} \right) I. \quad (8)$$

Since no radiation is incident from outside the ejecta the boundary conditions are:  $I^- = 0$  at the upper boundary and from symmetry at  $z = 0$ , the lower boundary condition is  $I^-(p, z) = I^+(p, z)$ . Integration of equation (8) gives:

$$\mathcal{I}(\tau_i) = \mathcal{I}(\tau_{i+1})e^{-\Delta\tau} + \int_{\tau_i}^{\tau_{i+1}} \frac{f_{rad}}{Y_e} e^{-(t-\tau_i)} dt \quad (9)$$

where  $\tau_i$  and  $\tau_{i+1}$  are the optical depths to points  $i, i+1$  along the ray and  $\Delta\tau = (\tau_{i+1} - \tau_i)$ . The impact parameter grid consists of rays tangent to concentric shells (Figure 1), with a single ray passing through the center. Since  $f_{rad}, Y_e$  are constant within each shell, equation (9) can be integrated exactly.

By setting  $\kappa_\nu = \kappa_{abs}^\nu$  we can calculate the rate ( $R_E$ ) at which the energy is deposited locally (in  $\text{erg cm}^{-3} \text{ s}^{-1}$ ) from:

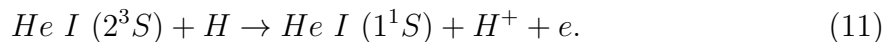
$$R_E = \sum_\nu 4\pi\kappa_\nu J_\nu \quad (10)$$

where  $J_\nu$  is the mean intensity of the  $\gamma$ -rays with initial energy  $E_\nu$ . The emergent luminosity of the individual (unscattered)  $\gamma$ -ray line photons can also be calculated with the  $\gamma$ -ray transport calculation described above by setting  $\kappa_\nu = N_e \times \sigma_{KN}(E_\nu)$  (Woosley *et al.* 1994).

## 2.2 Calculation of the He I 10830 Å line

In a H/He envelope of low ionisation, all the energy released by the Compton scattering of the  $\gamma$ -rays is channelled into ionisation of the H and He, rather than into heating the electron gas (Meyerott 1980). Thus, we assume the key populating process for the helium levels is recombination. We ignore direct excitation by fast electrons since they only excite singlet states, which decay rapidly back to the ground state. Of the recombinations to excited levels of He I, approximately three-quarters are to triplet states, with the remainder going to singlet states (Osterbrock 1989). Recombinations to singlet states cascade rapidly to the ground state. However, because there is a substantial optical depth in the  $1s^1S$ - $np^1P$  transitions (Graham 1988) all singlet recombinations will eventually pass through the  $2s^1S$  state. Atoms in the  $2s^1S$  level decay by two-photon emission ( $A=51 \text{ s}^{-1}$ ) to the ground state. Therefore, only a small population of excited singlet states is built up.

Recombinations to triplet states lead, through downward radiative transitions, to the highly metastable  $2s^3S$  level where the population can become quite substantial. As described in Fassia *et al.* (1998), there are a number of mechanisms which can depopulate this level. Firstly, a very weak single-photon radiative decay to  $1s^1S$  can occur ( $A = 1.27 \times 10^{-4} \text{ s}^{-1}$ ) (Osterbrock 1989). Of considerably greater significance, however, is the 2-stage intersystem radiative decay  $2s^3S \rightarrow 2p^3P \rightarrow 1s^1S$ . This occurs in the presence of a radiation field (such as from the photosphere), which is required to excite the first stage. There are also two important depopulating processes involving collisions. One of these involves thermal electron collisions causing excitation or de-excitation from  $2s^3S$  across to singlet states. The other process is Penning ionisation (Bell 1970, Chugai 1991):



which takes place when hydrogen and helium are microscopically mixed. Therefore, the population balance of the  $2s^3S$  level is described by the equation:

$$n_{\text{He}(2^3S)}(n_e Q + C_P + R + A) = \alpha(n^3L)n_e n_{\text{He II}}. \quad (12)$$

where  $Q$  is the sum of the collision rates from  $2s^3S$  to all singlet states, and has the value  $1.826 \times 10^{-8} \text{ cm}^3 \text{ s}^{-1}$  (Berrington & Kingston 1987).  $C_P$  is the Penning ionisation rate and is given by  $C_P = \gamma_P n_H$  where  $\gamma_P = 7.5 \times 10^{-10} (\frac{T}{300K})^{1/2} \text{ cm}^3 \text{ s}^{-1}$  (Bell 1970). For the recombination temperature of hydrogen ( $T \sim 5000 \text{ K}$ ), which we adopted for the days concerned (Catchpole *et al.* (1987)),  $\gamma_P = 3 \times 10^{-9} \text{ cm}^3 \text{ s}^{-1}$ .  $\alpha(n^3L) = 3.26 \times 10^{-13} \text{ cm}^3 \text{ s}^{-1}$  is the total recombination coefficient for the triplet states at a temperature of 5000 K (Osterbrock 1989).  $A$  is the spontaneous transition probability and  $R$  is the two stage inter-system radiative decay rate (Chugai 1991). This is given by:

$$R(\nu) = B_{23} \frac{4\pi}{c} \left(\frac{D}{vt}\right)^2 F_\nu^C e^{0.92A(\lambda)} A_{32}^{-1} A_{31} \beta_{31} \quad (13)$$

where  $\beta_{31}$  is the escape probability for the photon emitted in the decay  $2p^3P \rightarrow 1s^1S$  and  $F_\nu^C$  is the flux of the continuum at  $\lambda=10830 \text{ \AA}$ , determined from the observed infrared spectra.  $A(\lambda)$  is the extinction calculated using the empirical formula of Cardelli *et al.*

(1989) assuming  $A_V=0.6$  (Blanco *et al.* 1987). For the distance  $D$ , a value of 50 kpc was adopted.

For a deposition rate  $\epsilon_i$  ( $\text{erg cm}^{-3} \text{s}^{-1}$ ) in species  $i$ , the abundance of the next ionisation stage  $i+1$  is given by the energy balance :

$$n_{i+1} = \frac{\epsilon_i}{n_e \alpha_i w_i} \quad (14)$$

where  $n_e$  is the electron density,  $\alpha_i$  is the recombination rate to all levels of the species  $i$  and  $w_i$  is the energy required to produced an ion-electron pair. Considering an envelope that consists only of hydrogen and helium and taking the Penning ionisation into account, equation (14) reduces to:

$$\frac{\epsilon_H}{w_H} + n_{He(2^3S)} n_{H I} C_P = n_{H II} n_e \alpha_{H I} \quad (15)$$

$$\frac{\epsilon_{He}}{w_{He}} = n_{He II} n_e \alpha_{He} \quad (16)$$

where  $\epsilon = \epsilon_{He} + \epsilon_H$  is the energy deposited in the envelope. The ratio of the energy deposited in H and He is  $\epsilon_{He}/\epsilon_H = mY$ , where  $Y = n_{He}/n_H$ . From the Bethe-Bloch formula for energy loss of fast electrons in H/He material, we find  $m$  to be 1.7. Assuming  $n_e = n_{He II} + n_{H II}$  we can then calculate the population of the  $2s^3S$  level,  $n_{2s^3S}(R)$  as a function of radius,  $R$ , using equations (15), (16) and (12). This requires the energy deposition rate  $\epsilon(R)$  which we obtain from the radiative transport calculation described in 2.1, the total number density  $n_{tot}(R) = n_{He I}(R) + n_{H I}(R) + n_e(R)$ , and the relative abundance of hydrogen and helium,  $Y = \frac{n_{He II}(R) + n_{He I}(R)}{n_{H II}(R) + n_{H I}(R)}$ . The last two quantities were obtained from detailed explosion models.

The calculated density profile of the population of the  $2s^3S$  level,  $n_{2s^3S}(R)$ , was then fed into our spectral synthesis code (Fassia *et al.* 1998), thus producing a model He I 10830 Å P Cygni line profile. This was then compared with the observed profile.

### 3 Results

We first applied the technique described above to the radially-symmetric, unmixed model 10H (Woosley 1988). This model represents the explosion of a blue supergiant consisting of a  $6 M_\odot$  helium core, and a  $10 M_\odot$  hydrogen envelope. The model incorporated an explosion energy of  $1.4 \times 10^{51}$  ergs and a  $^{56}\text{Ni}$  mass of  $0.07 M_\odot$ . Among the *unmixed* explosion models, 10H was one of the most successful at reproducing the observed UVOIR light curve. Nevertheless, significant discrepancies existed. Model 10H also failed to explain the early detection of X-rays and  $\gamma$ -rays. Nor did it account for the high velocities observed in the iron-group line profiles. The present work shows (Figure 2a) that model 10H also fails to reproduce the pronounced He I absorption trough observed at  $\sim 10700$  Å. The lack of this He I trough means that the emission component of the C I 10695 Å line is unsuppressed resulting in a poor match to the



observed spectrum. This discrepancy is not surprising since, in 10H,  $^{56}\text{Ni}$  only extends to 1100 km/s (Figure 3), whereas at 76 days for example, the helium photosphere is at  $\sim 4700$  km/s. The  $\gamma$ -rays simply do not penetrate to sufficiently high velocities.

In order to account for the early detection of the X-rays and  $\gamma$ -rays Pinto & Woosley (1988) introduced *ad hoc* outward microscopic mixing into model 10H, yielding model 10HMM. In this model, radioactive material is mixed outwards through the helium core and into the hydrogen envelope. Model 10HMM successfully reproduced the UVOIR light curve and accounted for the early and prolonged detection of X-rays and  $\gamma$ -rays. However, on applying our technique to this model, we found that it provides a poor match to the observed He I 10830 Å line profile (Figure 2b). This is because the extensive dredge-up of  $^{56}\text{Ni}$  invoked in model 10HMM (Figure 3) produces a  $2s^3S$  population density that is much too high in the line forming region.

In order to attempt to match the observed line profile we repeated the microscopic mixing procedure that Pinto & Woosley applied to model 10H (Pinto, private communication). Turbulent or macroscopic mixing will be discussed in the next section. Starting from the centre, we specified a velocity interval and homogenized the material composition over that interval. We repeated this procedure, moving outwards until the edge of the ejecta was reached. This brings a fraction of the radioactive material to high velocities. Nevertheless, the abundance gradient is such that the bulk of the radioactive material remains at low velocities.

For each of the mixed models produced we calculated the  $\gamma$ -ray energy deposition, ionisation balance and  $2s^3S$  population density as a function of radius, and then compared the resulting synthetic He I 10830 Å line profile with the observations. Figure 3 shows the  $^{56}\text{Ni}$  distribution for two of our mixed models (denoted 10HMA and 10HMB) that provided a good match to the observed He I 10830 Å line profile. The synthetic helium line profiles deduced using model 10HMB are compared with the observations in Figure 4. Equally good fits were obtained for model 10HMA.

We also modelled the  $\gamma$ -ray line light curves for models 10HMA and 10HMB using the radiative transport calculation explained in 2.1 and adopting  $\kappa_\nu = N_e \times \sigma_{KN}(E_0)$ . In Figure 5, these light curves are compared with  $\gamma$ -ray observations (Leising & Share 1990; Sandie *et al.* 1988), assuming a distance of 50 kpc. Also shown are the  $\gamma$ -ray light curves deduced using model 10HMM.

## 4 Discussion

The results show that we can reproduce the He I line by reducing the amount of microscopic mixing that was invoked in model 10HMM. Indeed, in model 10HMA there was negligible radioactive material at velocities exceeding  $\sim 3,900$  km/s. This is in contrast with 10HMM where  $\sim 1\%$  of the total  $^{56}\text{Ni}$  mass has velocities in excess of 3,900 km/s. We find better agreement with the more recent work of Nomoto *et al.* (1998). Based on their explosion model 14E13, their bolometric light curve calculations

suggest that  $^{56}\text{Ni}$  is mixed up to 3,000–4,000 km/s.

For models 10HMA and 10HMB we find that, respectively, 4% and 3% of the total  $^{56}\text{Ni}$  mass ( $0.07 M_{\odot}$ ) lay above 3,000 km/s. This is consistent with late-time infrared spectroscopic observations which showed that a small fraction of the cobalt and iron was travelling at velocities  $\sim 3,000$  km/s (Spyromilio, Meikle & Allen 1990; Haas *et al.* 1990; Tueller *et al.* 1990). From their 18  $\mu\text{m}$  and 26  $\mu\text{m}$  [Fe II] line profiles, Haas *et al.* inferred that  $\geq 4\%$  of the iron mass had an expansion velocity greater than 3,000 km/s. We also note that  $\gamma$ -ray light curve predictions based on models 10HMA and 10HMB are consistent with the observations (Figure 5).

Models 10HMM, 10HMA and 10HMB are equally successful at accounting for the  $\gamma$ -ray light curves and late-time infrared line velocities. However, in reproducing the observed early-time He I 10830  $\text{\AA}$  line, models 10HMA and 10HMB are clearly superior to 10HMM. We conclude that, given current technology, the He I line technique provides a better measure of the dredge-up of radioactive materials in type II supernovae. Some of the advantage of the He I line method stems from the fact that it uses near-IR observations taken at relatively early times when the supernova is bright. An additional advantage is that, since the method is based primarily on the optical depth of the He I P Cygni line, it is insensitive to fluxing errors (Fassia *et al.* 1998).

In the above work, microscopic mixing was assumed, and so Penning ionisation dominated the depopulation of the  $2s^3\text{S}$  level (*cf* Fassia *et al.* 1998). However, hydrodynamic calculations show that mixing is turbulent and takes place on macroscopic length scales. Multi-dimensional studies predict that hydrogen and helium bubbles will be dragged towards the inner parts of the ejecta, while clumps of helium and heavier elements, including radioactive nickel, will penetrate the hydrogen envelope (Fryxell, Müller and Arnett 1991, Herant & Benz 1991). Pure helium clumps in the hydrogen envelope will tend to dominate the population of the  $2s^3\text{S}$  level as they are not subject to the effects of Penning ionisation. Helium that is microscopically mixed with hydrogen will make a negligible contribution even if its abundance is much greater. In Fassia *et al.* (1998) we demonstrated that the presence of helium clumps in the hydrogen envelope *reduces* significantly the degree of  $^{56}\text{Ni}$  dredge-up that is needed to drive the He I 10830  $\text{\AA}$  line. In that study we assumed that the  $^{56}\text{Ni}$  was microscopically mixed with the helium bubbles and the hydrogen envelope. However, in the case of SN 1987A, there is good evidence that some of the  $^{56}\text{Ni}$  was ejected in fast-moving clumps (*e.g.* Spyromilio, Meikle & Allen 1990). Thus, if the  $^{56}\text{Ni}$  in the vicinity of the He I line forming region is not microscopically mixed, it may be necessary to *increase* the degree of  $^{56}\text{Ni}$  dredge-up to provide the required rate of helium ionisation. Clearly, this is a complicated problem, requiring the use of 2-D and 3-D explosion models. We therefore defer to a later paper an examination of the implications of macroscopic mixing in SN 1987A for the He I technique. This should ultimately allow us to place constraints on the initial inhomogeneities.

Finally, we note that the He I observations take place well before the  $\gamma$ -ray lines reach maximum brightness. Thus, by observing the He I 10830  $\text{\AA}$  line in type II supernovae at early times, we should be able to make accurate predictions of the  $\gamma$ -ray fluxes,

providing a valuable “early-warning” facility for  $\gamma$ -ray observers.

## Acknowledgments

We thank Phil Pinto and Stan Woosley for their advice and the use of their explosion models. AF is supported by a scholarship from the Alexander S Onassis Public Benefit Foundation.

## References

- Arnett W. D., 1988, ApJ, 331, 337  
Arnett W.D., Fryxell B.A., Müller E., 1989, ApJL, 341, L63  
Arnett W. D., 1994, ApJ, 427, 932  
Bandiera R., 1984, A&A, 139, 368  
Bazan G., Arnett, D., 1998, ApJ, 496, 316  
Bell K.L., 1970, J.Phys.B:Atom.Molec.Phys., 3, 1308  
Berrington K. A., Kingston A. E., 1987, J. Phys. B: Atom. Molec. Phys., 20, 6631  
Blanco MV. M., Gregory B., Hamuy M., Heathcote S. R., Phillips M. M., Suntzeff N. B., Terndrup D. M., Walker A. R., Willieams R. E., Pastoriza M. G., Storch-Bergmann T., Matthews J., 1987, ApJ 320, 589  
Cardelli J., Clayton G., Maths J., 1989, ApJ, 345, 245  
Catchpole R. M., Menzies J. W., Monk A. S., Wargau W. F., Pollacco D., Carter B. S., Whitelock P.A., Marang F., Laney C. D., Balona L. A., Feast M. W., Lloyd Evans T. H. H., Sekiguchi K., Laing J. D., Kilkenny D. M., Spencer Jones J., Roberts G., Cousins A. W.J., van Vuuren G., Winkler H., 1987, MNRAS, 229, 15  
Chevalier R.A., 1976, ApJ, 207, 872  
Chugai N.N., 1991, in Supernovae, ed. Woosley S.E., Springer-Verlay, New York, p286  
Cook W. R.,Palmer D. M., Prince T. A., Schindler S. M., Starr C. H., Stone E. C., 1988, ApJ, 334, L87  
Dotani T., Hayashida K., Inoue H., Itoh M., Koyama K., 1987, Nature, 330, 230  
Elias J.H., Gregory B., Philips M.M., Williams R.E., Graham J.R., Meikle W.P.S., Schwartz R.D., Wilking B., 1988, ApJ, 331, L9  
Falk S.W., Arnett D.W., 1973, ApJ, 180, L65  
Fassia A., Meikle W. P.S., Geballe T. R., Walton N. A., Pollacco D. L., Rutten R. G. M., Tinney C., 1998, MNRAS, in press  
Fryxell B, Arnett W. D., Müller E., 1991, ApJ, 367, 619  
Graham J.R., 1988, ApJ, 335, L53  
Haas M. R., Colgan S. W. J., Erickson E. F., Lord S. D., Burton M. G., Hollenbach D. J., 1990, ApJ, 360, 257  
Hachisu I., Matsuda T., Nomoto K., Shigeyama T., 1990, ApJ, 358, L57

Herant M., Benz W., 1991, ApJ, 345, L412  
 Herant M., Benz W., 1992, ApJ, 387, 294  
 Herant M., Benz W., Colgate S., 1992, ApJ, 395, 642  
 Herant & Woosley , 1994, ApJ, 425, 814  
 Herant M., Benz W., Hix R. W., Fryer C. L., Colgate S. A., 1994, ApJ, 435, 339  
 Lederer C. M., Shirley V. S., 1978, *Table of Isotopes* (7th ed. New York: Wiley)  
 Leising M. D., Share G. H., 1990, ApJ, 357, 638  
 Mahoney W. A., Varnell L. S., Jacobson A. S., Ling J.C., Radocinski R. G.,  
 Wheaton WM. A., 1988, ApJL334, L81  
 Matz S. M., Share G. H., Leising M. D., Chupp E. L., Vestrand W. T., Purcell W.  
 R., Strickman M. S., Reppin C., 1988, Nature, 331, 416  
 Meikle W.P.S., Allen D.A., Spyromilio J., Varani G.-F., 1989, MNRAS, 238, 193  
 Meyerott R.E., 1980, in *Supernovae Spectra*, ed. R.E. Meyerott and G.H. Gillespie  
 (AIP Conf. Proc. 63), p49  
 Müller E., Fryxell B., Arnett W. D., 1991, A&A, 251, 505  
 Nomoto K., Blinnikov S.I., Iwamoto, K., 1998, in Proc. 1st CTIO/ESO/LCO  
 Workshop: *SN 1987A: TEN YEARS AFTER*, eds. M.M. Phillips & N.B. Suntzeff,  
 publ. Ast. Soc. Pac. (in press)  
 Osterbrock D.E., 1989, in *Astrophysics of Gaseous Nebulae and Active Galactic  
 Nuclei*, p25  
 Pinto P. A., Woosley S. E., 1988, Nature, 333, 534  
 Sandie W.G. , Nakano G. H., Chase L. F., Fishman G. J., Meegan C. A., Wilson  
 R. B., Paciasas W. S., Lasche G. P., 1988, ApJ, 334, L91  
 Shigeyama T., Nomoto K., Hashimoto M., 1988, A&A, 196, 141  
 Shigeyama T., Nomoto K., 1990, ApJ, 360, 242  
 Spyromilio J., Meikle W. P. S., Allen D. A., 1990, MNRAS, 242, 669  
 Sunyaev R. A., Kaniovsky A., Efremov V., Gilfanov M., Dhurazov E., Grebenev  
 S. A., Kuznetsov A. V., Melioranskii A. S., Yamburenko N. S., Yunin S., Stepanov  
 D., Chulkov I, Pappé N., Boyarskii M. N., Gavrilova E. A., Loznikov V. M., Prud-  
 koglyad A., Rodin V. G., Reppin C., Pietsch W., Engelhauser J., Trumper J.,  
 Voges W., Kendziorra E., Bezler M., Staubert R., Brinkman A. C., Heise J., Mels  
 W. A., Jager R., Skinner G. K., Al-Emam O., Patterson T. G., Willmore A. P.,  
 1987, Nature, 330, 227  
 Swartz D. A., Sutherland P. G., Harkness R. P., 1995, ApJ, 446, 766  
 Tueller J, Barthelemy S., Gerhels N., Teegarden B. J., Leventhal M., MacCallum  
 C. J., 1990, ApJ, 351, L41  
 Woosley S. E., 1988, ApJ, 330,218  
 Woosley S. E., Eastman R. G., Weaver T. A., Pinto P. A., 1994, ApJ, 492, 300

## Figure Captions

Figure 1 : The coordinate system (p,z) used for the radiative transfer calculation. The dashed line shows an example of an impact parameter ray along which the frequency dependent equations of transfer were integrated.

Figure 2 : Comparison of observed spectra of SN 1987A at 105 days, with synthetic spectra whose He I 10830 Å line profiles are based on models 10H and 10HMM. Data are from Elias *et al.* (1988).

Figure 3 : Distributions of  $^{56}\text{Ni}$  for models 10H (dashed line), 10HMM (dotted line), 10HMA (solid line) and 10HMB (dot-dashed line).

Figure 4 : Comparison of observed spectra with synthetic spectra whose He I 10830 Å line profiles are based on model 10HMB. Data are from Elias *et al.* (1988) and Meikle *et al.* (1989).

Figure 5 : Comparison of the  $\gamma$ -ray line light curves of model 10HMA (solid line) and model 10HMB (dotted line) with the observations. Data are from Leising & Share (1990) (open triangles) and from Sandie *et al.*(1988) (open squares). The dashed line represents the predictions of model 10HMM.

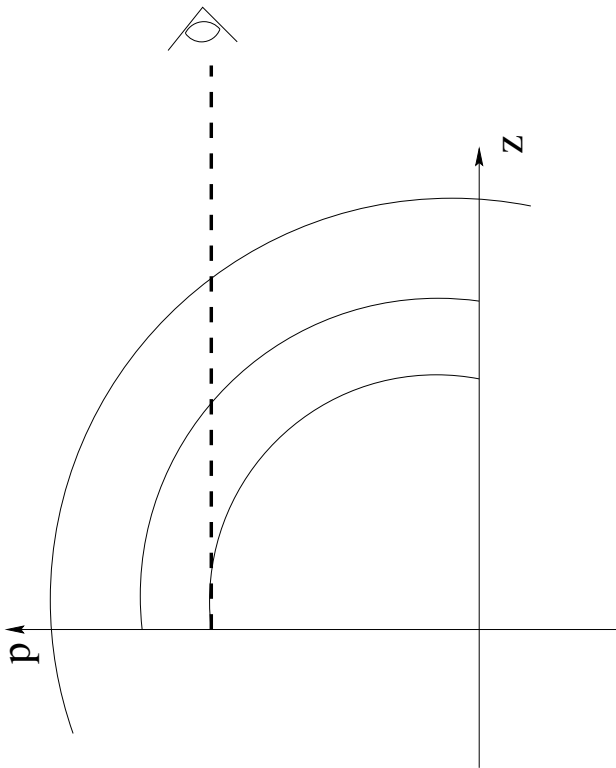


Figure 1:

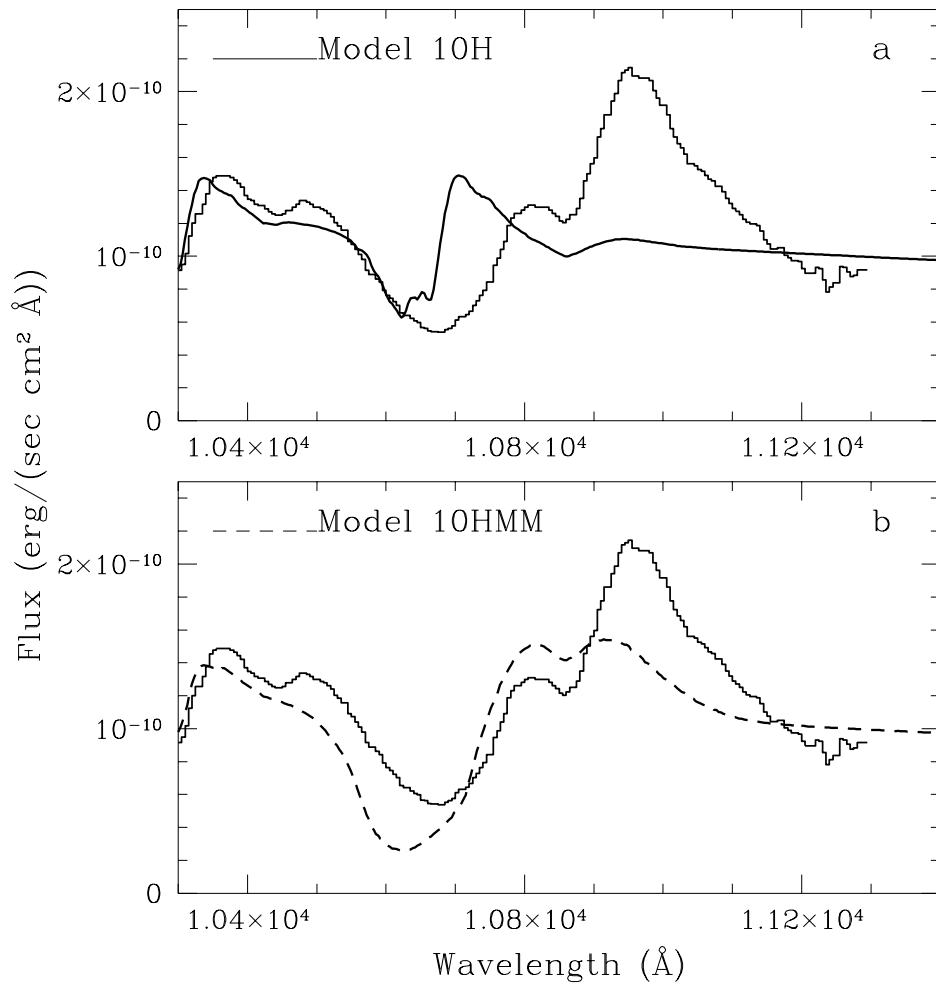


Figure 2:

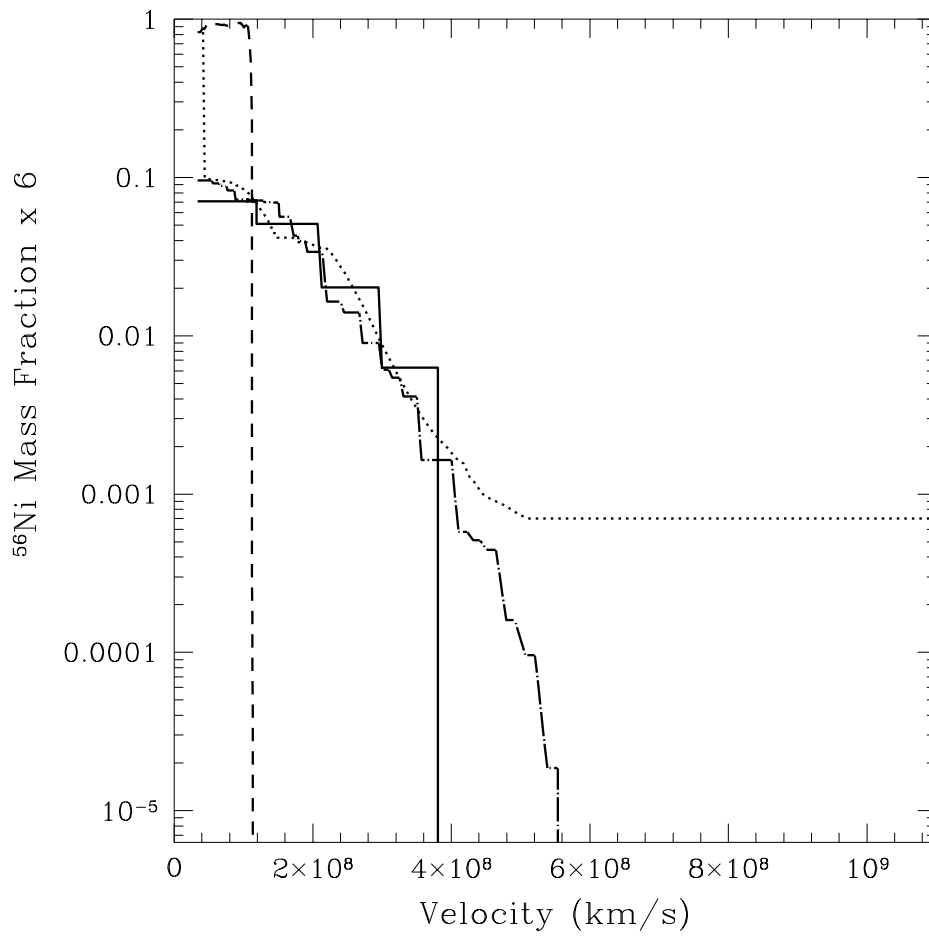


Figure 3:



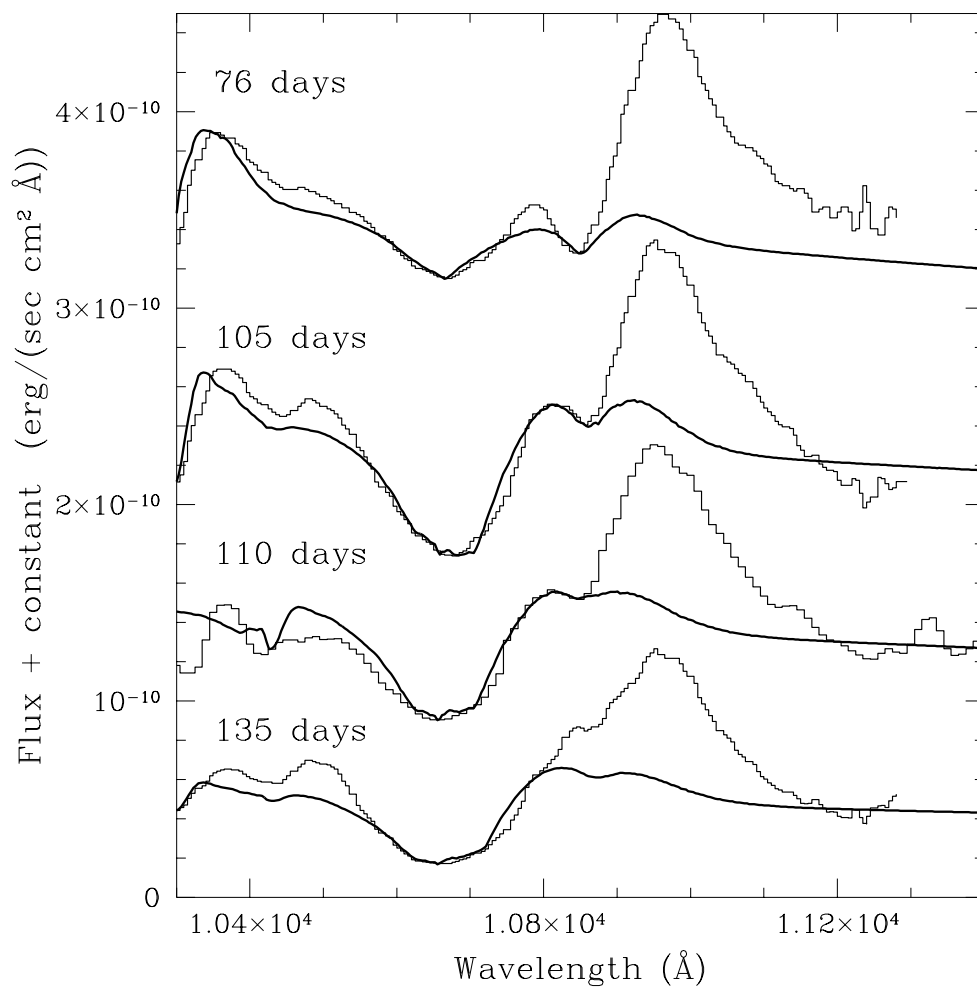


Figure 4:

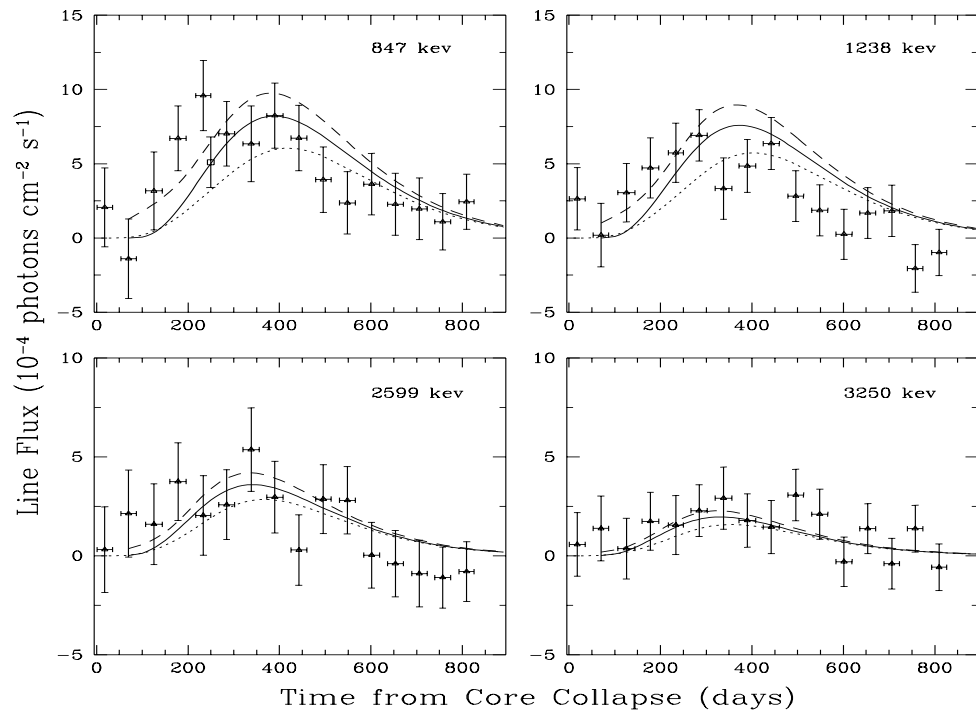


Figure 5: